Applied Catalysis B: Environmental 254 (2019) 66–75

Contents lists available at ScienceDirect

Applied Catalysis B: Environmental

journal homepage: www.elsevier.com/locate/apcatb

Magnetically separable TiO_2/FeOx/POM accelerating the photocatalytic removal of the emerging endocrine disruptor: 2,4-dichlorophenol

Jiajie Yu[a,b], Tianhe Wang[b], Sami Rtimi[a,*]

[a] Ecole Polytechnique Federale de Lausanne, EPFL-ISIC-GPAO, Station 6, 1015, Lausanne, Switzerland
[b] Chemicobiology and Functional Materials Institute, Nanjing University of Science and Technology, Nanjing, 210094, PR China

ARTICLE INFO

Keywords:
2,4-Dichlorophenol (2,4-DCP)
Photo-degradation
TiO_2/FeOx/POM
Magnetic
Interfacial charge transfer (IFCT)
TiO_2-FeOx intra-gap states

ABSTRACT

This study presents the magnetically separable TiO_2/FeOx microstructure decorated with poly-oxo-tungstate (POM) leading to the endocrine disruptor 2,4-dichlorophenol (2,4-DCP) under low intensity solar light. The fastest 2,4-DCP degradation kinetics was obtained by way of the TiO_2/FeOx(25%)/POM(1%) composite in acidic media. The use of magnetized photocatalysts avoids the high cost separation of the catalysts from the solution by conventional treatments after 2,4-DCP-degradation. Reactive oxygen species (ROS) leading to the 2,4-DCP degradation were identified by use of appropriate scavengers. The 2,4-DCP degradation increased with the applied light intensity (fluence rate) providing evidence for the semiconductor behavior of the composite material. FeOx/Fe_2O_3 intra-gap states were identified by X-ray photoelectron spectroscopy (XPS) leading to 2,4-DCP degradation. A scheme for the interfacial charge transfer (IFCT) between the oxides is suggested based on the electronic energy position of the oxides making up the photocatalytic composite.

1. Introduction

2,4-Dichlorophenol (2,4-DCP), one of the typical chlorophenols, is a common non-biodegradable organic contaminant in waste water and drinking water. It has been widely used as pesticides, herbicides, germicides and preservatives and can also be formed as a result of degradation and metabolism of agricultural and food chemicals [1–3]. It is a precursor for the synthesis of carcinogenic 2,4-dichlorophenoxyacetic acid (an endocrine disruptor) [4]. The 2,4-DCP has been shown to cause endocrine related cancers. Even in an extremely low concentration of 2, 4-DCP, it would cause huge damage to organisms and environment [5].Several strategies such as adsorption, advanced oxidized processes (AOPs) and photocatalysis have been applied to eliminate 2,4-DCP from water [6–8]. By AOPs, 2,4-2,4-DCP has been removed by ferrioxalate/H_2O_2 [2], iron/persulfate [9] and H_2O_2/UV-C systems [10]. Photocatalysis is one of the most promising techniques allowing efficient degradation of pollutants in a cost-effective and environmentally friendly way [11]. N. Serpone et al. investigated the kinetics of TiO_2 mediated photodegradation of 2,4-dichlorophenol [12]. Nanoscale Fe/TiO_2 was prepared by L. Liu et al. using a sol-gel method followed by reductive deposition of Fe and tested for 2,4-DCP photocatalytic degradation [13].

Since the photosensitization effect of TiO_2 photoelectrode was reported by A. Fujishima and K. Honda in 1972 [14], TiO_2 has received considerable attention due to its strong redox ability, low cost, non-toxicity, high stability and widespread availability [15,16]. TiO_2 can be prepared with large specific surface area, enhancing the photocatalytic performance of this material. However, the practical application of TiO_2 is often restricted due to the problems associated with charges recombination and a large band gap of ~3.3 eV, leading to inefficient utilization of solar light. Efforts have been made to reduce the charge-recombination of TiO_2 [17–19]. Polyoxometalates (POMs) are a vast class of transition oxygen-bridged metal clusters anions of tungsten and molybdenum presenting properties as semiconductors [20]. POMs have received considerable attention over the past few decades due to their non-toxic, inexpensive and strong oxidative properties [21]. POMs have been employed as electron scavengers in combination with TiO_2 to decrease charge the later recombination, leading to a significant enhancement of the photodegradation rates. Ozer et al., showed that the addition of POM anions to TiO_2 dispersion significantly enhanced the photo-oxidation of dichlorobenzene [22]. J. J. Zhao reported the intermediates and mechanism for accelerating 2,4-DCP degradation by TiO_2 dispersion in the presence of POM [23]. POMs have been mostly used in homogeneous solution to TiO_2-dispersions. In this case, the TiO_2 dispersion has to be separated/ from the solution by centrifugation and/or ultra-filtration at the end of the treatment. This requires labor, time, energy input and high costs. FeOx-based photocatalysts precludes the costly separation and extends the response of TiO_2 into the visible

* Corresponding author.
E-mail address: sami.rtimi@epfl.ch (S. Rtimi).

https://doi.org/10.1016/j.apcatb.2019.04.088
Received 13 March 2019; Received in revised form 19 April 2019; Accepted 25 April 2019
Available online 27 April 2019

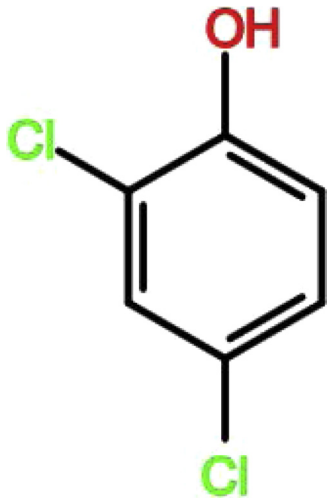

Scheme 1. Chemical structure of the 2,4-DCP.

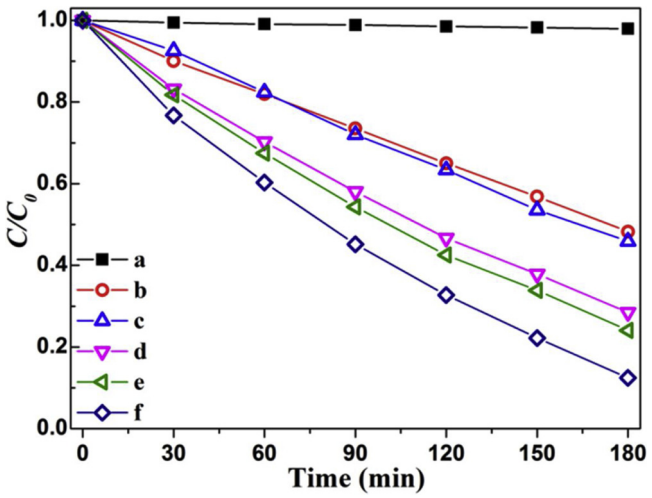

Fig. 1. Degradation of 50 mL 2,4-dichlorphenol (2,4-DCP) on the following: (a) TiO_2/FeOx(25%)/POM(1%) in the dark, (b) TiO_2, (c) TiO_2/FeOx(25%), (d) TiO_2/POM(1%)/FeOx(25%), (e) TiO_2/FeOx(25%)/POM(1%) and (f) TiO_2/POM (1%) under simulated solar light. Solution parameters: [catalyst] = 500 mg/L, [2,4-DCP] = 10 mg/L, initial pH 5.0, solar light intensity (fluence rate) 48.9 mW/cm^2.

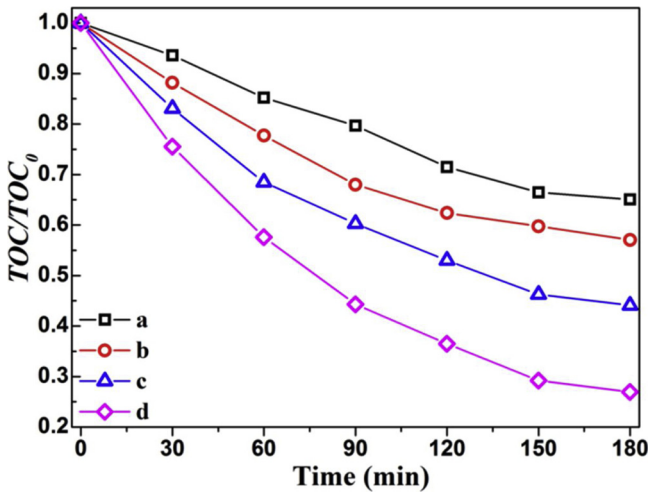

Fig. 2. TOC removal of 2,4-dichlorphenol (2,4-DCP) on the following samples: (a) TiO_2, (b) TiO_2/FeOx(25%), (c) TiO_2/FeOx(25%)/POM(1%) and (d) TiO_2/POM(1%) under simulated solar light. Solution parameters: [catalyst] = 500 mg/L, [2,4-DCP] = 10 mg/L, pH 5.0, solar light intensity (fluence rate) 48.9 mW/cm^2.

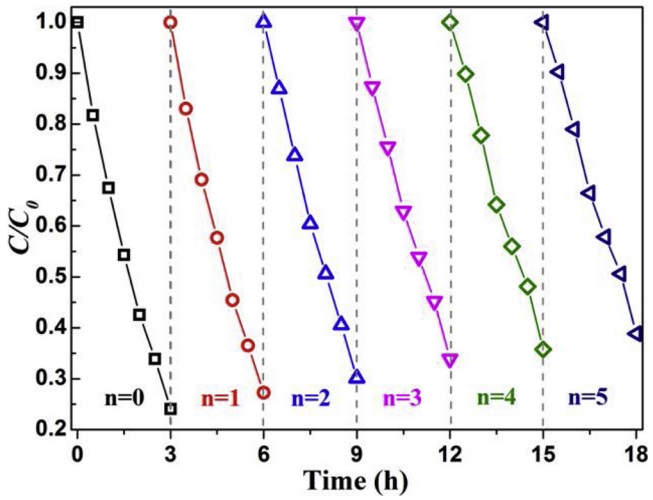

Fig. 3. Five 2,4-DCP-degradation cycles catalyzed by TiO_2/FeOx(25%)/POM (1%) under simulated solar light. Solution parameters: [catalyst] = 500 mg/L, [2,4-DCP] = 10 mg/L, pH 5.0, solar light intensity 48.9 mW/cm^2.

region.

This study presents an innovative magnetically separable TiO_2/FeOx/POM leading to DC-degradation under light irradiation. We report the details of the preparation and surface properties macro-sized of TiO_2/FeOx/POM by mean of XRD, XRF, XPS and SEM. The performance of TiO_2/FeOx/POM leading to 2,4-DCP degradation has been investigated evaluating the catalyst dosage, the effect of the applied light intensity and the type of light applied. A scheme for the interfacial charge transfer (IFCT) is suggested based on the position of the electronic potential energies of the oxides making up the photocatalyst.

2. Experimental

2.1. Materials preparation

The preparation of TiO_2 follows hydrothermal method by Kasuga et al [24] being modified to improve the photocatalyst 2,4-DCP degradation. In a brief, TiO_2 (P25 aerosol, Evonik) were added in de-ionized water stirring for 4 h to obtain the suspension (2 g/L). The dispersion was introduced into a Teflon vessel with 10 M NaOH aqueous solution, then placed in stainless steel vessel and heated at 110 °C for 20 h. The obtained material was washed with 10% HCl and de-ionized water, and then centrifuged. This process was repeated until the solution reached a pH < 7.

For the preparation of the TiO_2/FeOx(25%) sample, 50 mL of deionized water was added in a beaker and purged continuously with N_2 air. Then 29.5 mg of $FeCl_2{\cdot}4H_2O$ (Sigma Aldrich) and 80.5 mg of $FeCl_3{\cdot}6H_2O$ in a [Fe^{2+}] : [Fe^{3+}] molar ratio of 1:2. Then 1 mL of NH_3 (Merck, 25%) and 100 mg as-prepared TiO_2 were added to the black precipitate, while stirring at 85 °C in a water bath for 45 min. Finally, the products were harvested with a magnet and washed repeatedly with deionized water. The resulting powders were oven dried at 70 °C for 3 h before storing.

TiO_2/FeOx/POM were prepared in the following way: POM synthesis was carried out according to reference [25]. The POM was added with mechanic stirring for 20 h on TiO_2/FeOx washed with water and ethanol for several times, centrifuged and dried. TiO_2/ FeOx(25%)/POM(1%) composite was prepared in a similar way except that the preparation sequence of FeOx and POM was inversed.

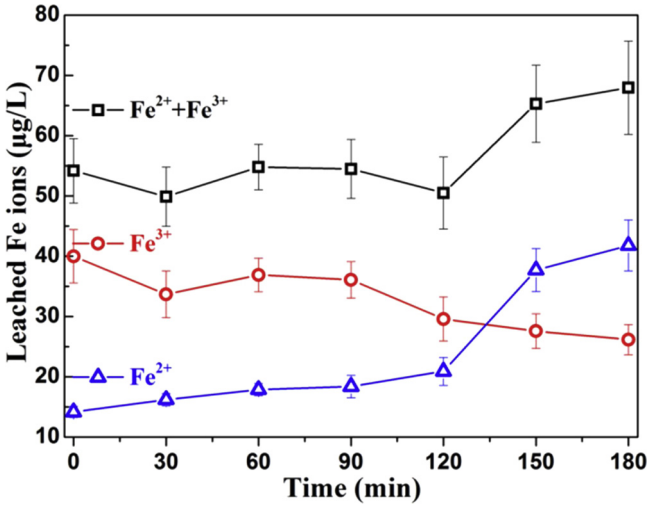

Fig. 4. Evaluation of Fe ions leaching during 2,4-DCP degradation mediated by TiO_2/FeOx(25%)/POM(1%) under simulated solar light. Solution parameters: [catalyst] = 500 mg/L, [2,4-DCP] = 10 mg/L, pH 5.0, solar light intensity 48.9 mW/cm^2.

2.2. Photocatalytic degradation of 2,4-DCP, irradiation set-up and scavenging of the reactive oxygen species (ROS)

The photo-degradation of 2,4-DCP (Scheme 1) was carried out in the cavity of a Suntest solar simulator CPS (Atlas GmbH, Hanau, Germany). In a typical run, 25 mg of the photocatalyst was placed in a 50 mL photochemical reactor with 10 mg/L 2,4-DCP. The pH of the pollutant solution was adjusted by 0.1 M NaOH or 0.1 M HCl aqueous solution (see Fig. 1). At pre-selected times, 2 mL aliquots were withdrawn to evaluate the 2,4-DCP-degradation kinetics. The concentration of 2,4-DCP was determined by the high-pressure liquid chromatography (HPLC). For the runs monitored in the visible light irradiation, a cut-off filter ($\lambda > 410$ nm) was added to the solar simulator. The effect of the light in the Suntest simulator was carried out varying the power applied to the Xe-light source. The light intensity was monitored using a UV radiometer and a global irradiance couple (CUV3 and CM3 Models, from Kipp & Zonen). The term "light intensity" (or fluence rate) is used based on the definition reported in reference [26].

Scavenging experiment were investigated to determine the reactive oxygen species (ROS) using p-benzoquninone as $HO_2^{-\cdot}$ radical scavengers; NaN_3 as the singlet oxygen $^1O_2$ scavengers; methanol as $^{\cdot}OH$ radical scavengers and EDTA-2Na as the vb-holes ($vbh^{\pm}$) scavengers [27,28]. The 2,4-DCP structural formula is given below (Scheme 1):

After the photocatalytic degradation, the TiO_2/ FeOx(25%)/POM (1%) photocatalyst was recovered with a magnet, washed with deionized water then oven dried at 70 °C for 3 h before subsequent reuse in another photocatalytic test.

2.3. Monitoring of the 2,4-DCP degradation by HPLC

High pressure liquid chromatography (HPLC) was performed on an Agilent 1100 instrument equipped with a C18 column (Superlcosil LC-18, 5 μm particle size, length 15 cm, i.d. 3 mm) with UV detector ($\lambda = 280$ nm). 20 μL 2,4-DCP solution was injected into the HPLC with a mobile phase consisting of acetonitrile and 0.1% formic acid solution in a ratio of 70:30 at a flow rate of 0.85 mL/min (25 °C).

2.4. Catalyst surface characterization

The morphology observation was conducted with a field-emission scanning electron microscopy (FESEM, S4800) operated at 20 kV. The TEM images of the catalysts were acquired on Quant 250FEG at 20 kV. Diffuse reflectance spectroscopy (DRS) of the prepared photocatalysts was performed on a PerkinElmer Lambda 950 UV–vis-NIR spectrometer

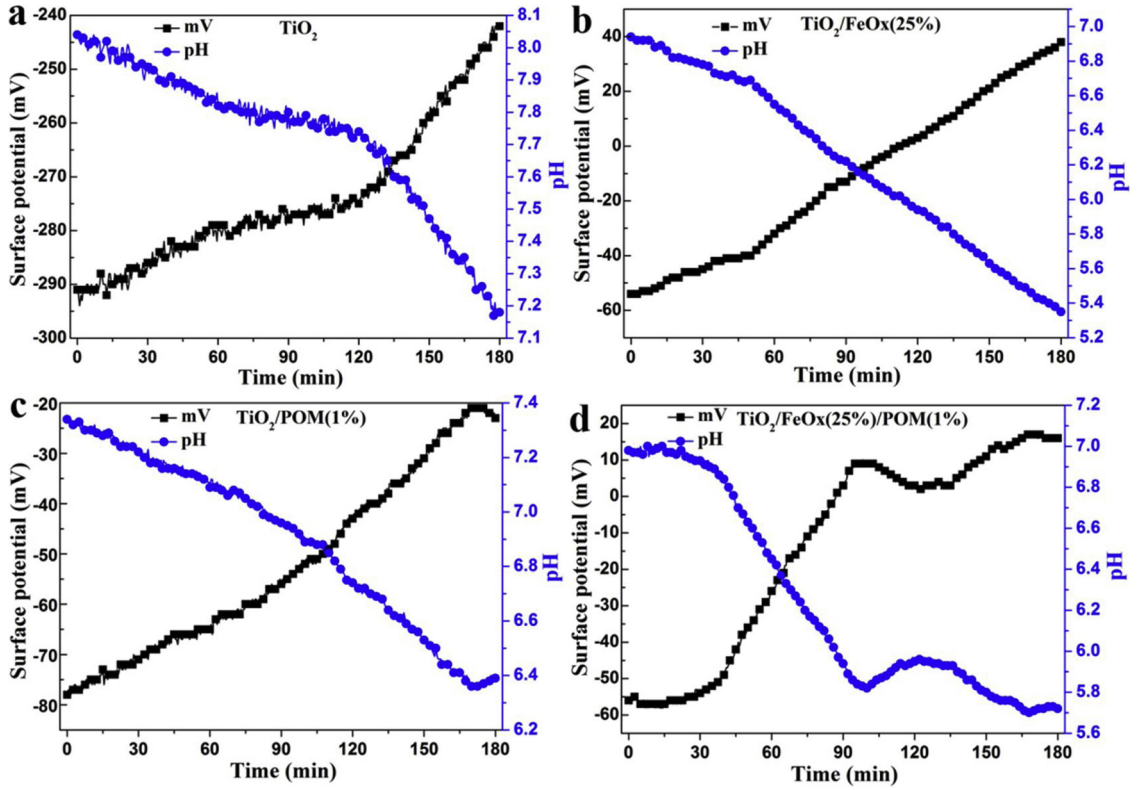

Fig. 5. Surface potential and local pH of (a) TiO_2, (b) TiO_2/FeOx(25%), (c) TiO_2/POM(1%) and (d) TiO_2/FeOx(25%)/POM(1%) under simulated solar light. Solution parameters: [catalyst] = 500 mg/L, [2,4-DCP] = 10 mg/L, solution pH 5.0 (before adding the catalysts), solar light intensity 48.9 mW/cm^2.

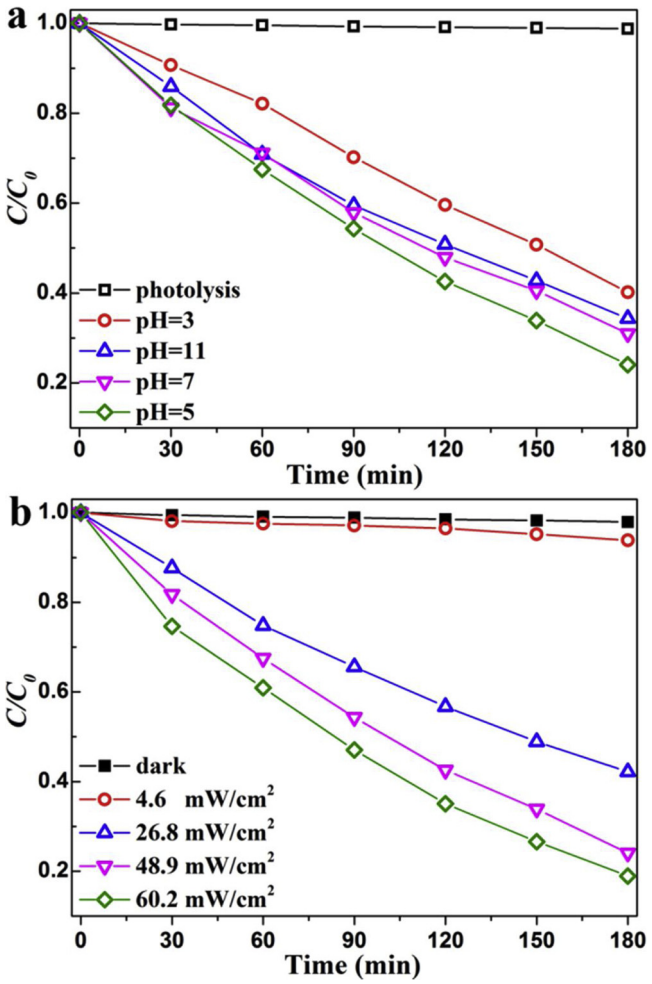

Fig. 6. Effect of (a) solution pH on the DC degradation kinetics. Solution parameters: [catalyst] = 500 mg/L, [2,4-DCP] = 10 mg/L, solar light intensity 48.9 mW/cm^2 and (b) light intensity. Solution parameters: [catalyst] = 500 mg/L, [2,4-DCP] = 10 mg/L and pH 5.0) for 2,4-DCP degradation mediated by TiO_2/FeOx(25%)/POM(1%).

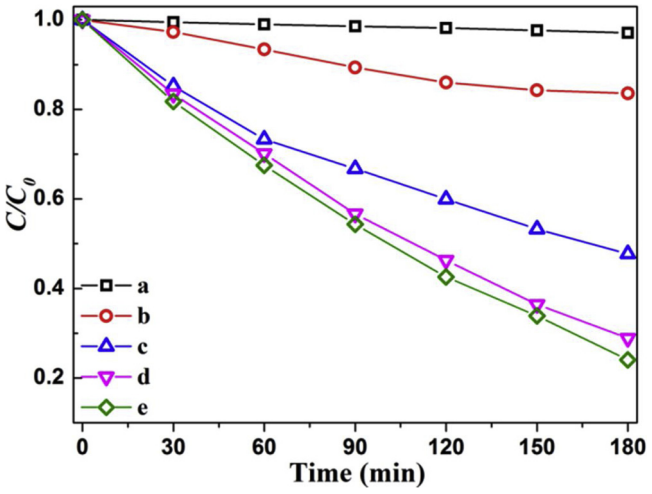

Fig. 7. Effect of ROS scavengers during 2,4-DCP degradation by TiO_2/FeOx (25%)/POM(1%) under simulated solar light: (a) 0.5 mM methanol, (b) 0.5 mM p-benzoquninone, (c) 0.5 mM NaN_3, (d) 0.5 mM KI and (e) no scavengers.

in the range of 250 nm to 800 nm. The samples were diluted in MgO and compressed as pellets before tests. X-ray diffraction (XRD)

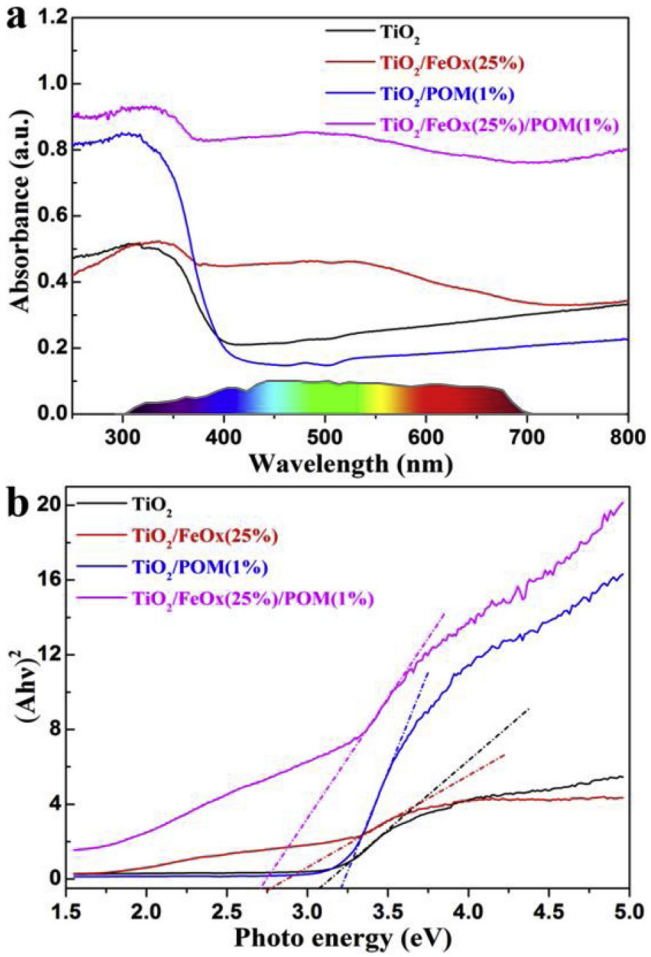

Fig. 8. (a) UV–vis spectra and (b) bandgap energies of: TiO_2, TiO_2/FeOx(25%), TiO_2/POM(1%) and TiO_2/FeOx(25%)/POM(1%). Spectral emission of the used solar simulated light is inserted in 8a.

measurement were operated on an X'Pert MPD PRO from PANalytical equipped with a secondary graphite (002) monochromator and a PIXcel-1D detector operated in Bragg-Brentano geometry. In order to measure the magnetic behavior of the prepared photocatalysts, the TiO_2-FeOx and the TiO_2/FeOx(25%)/POM(1%) samples were mixed with a diluted GE-varnish and measured at 300 K in the field-sweep sequence 0T→5T→-5T→5 T in a NPMS-Xl-5T-SQUID magnetometer. The specific surface areas (SSA) were obtained by Brunauer-Emmett-Teller (BET) analysis performed with a BELSORP-mini instrument.

The surface atomic percentage and chemical states of the element in the TiO_2/FeOx(25%)/POM(1%) before and after reuse were determined by X-ray photoelectron spectroscopy (XPS). An AXIS NOVA photoelectron spectrometer (Kratos Analytical, Manchester, UK) provided for with monochromatic AlK ($h\nu$ = 1486.6 eV) anode. Binding energies (BE) were calibrated against the standard C1 s binding energy at 284.8 eV [29,30]. Spectra were deconvoluted by means of a Multipak (version 9 software) using Gaussian: Lorentzian peak shape and a Shirley background function [31].

3. Results and discussion

3.1. Photodegradation of 2,4-DCP and optimization of photocatalyst

The effect of POM amount added to TiO_2 was investigated. The results are reported in the supplemental Figure S1. POM 1% added to the TiO_2 led to the fastest 2,4-DCP-degradation. POM scavenges electrons from the conduction band of TiO_2 to decrease the charge

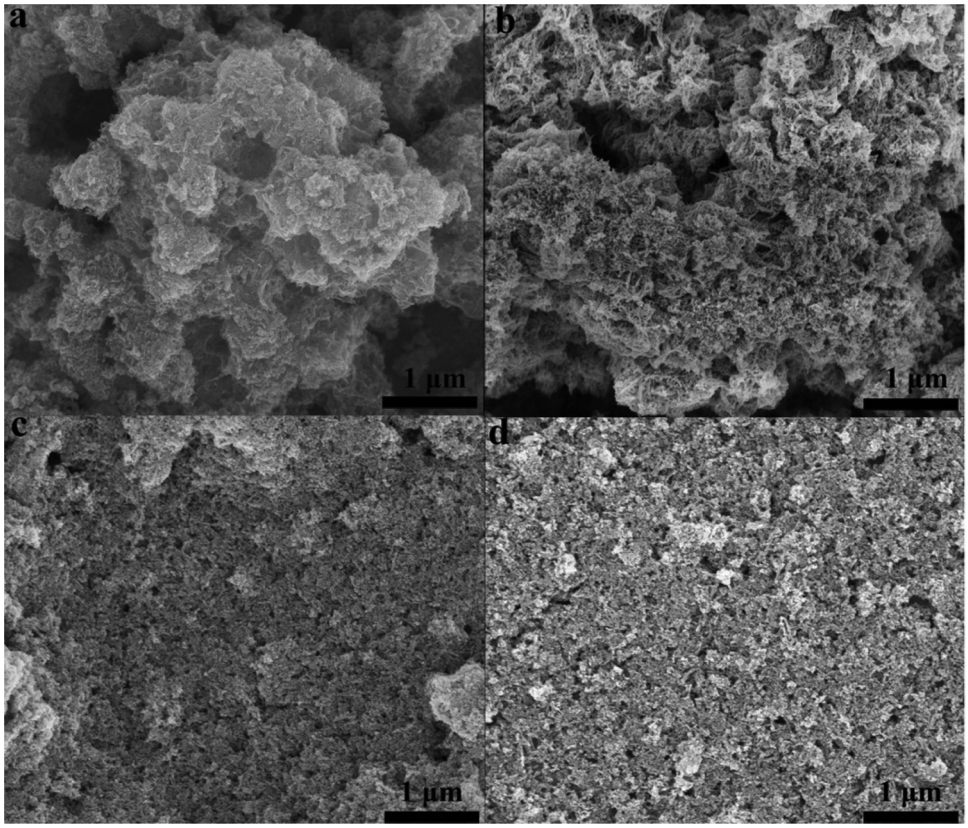

Fig. 9. SEM images of: (a) micro-sized TiO_2, (b) TiO_2/POM(1%), (c) TiO_2/FeOx(25%) and (d) TiO_2/FeOx(25%)/POM(1%).

recombination, thus enhancing the photocatalytic efficiency of TiO_2. The 1% limit was probable for the competition for the catalytic sites between TiO_2 and POM. A similar observation was found by Ozer and coworkers [22]. Supplemental Figure S2 shows that the incorporation of FeOx in TiO_2 lead to a slower 2,4-DCP-degradation except when the FeOx amount was 25%. The visible light used was in the optical absorption range of the FeOx/Fe_2O_3 (band-gap 2.2 eV) [32,33]. Electrons were promoted from the Fe_2O_3vb to the Fe_2O_3cb. Fig. 1 presents the photodegradation of 2,4-DCP on different samples under simulated solar light at pH 5.0. TiO_2/POM(1%) led to the fastest kinetics with 87.6% 2,4-DCP removal within 180 min, as shown in Fig. 1, trace a). However, only 76.0% 2,4-DCP was eliminated by TiO_2/FeOx(25%)/POM(1%). Considering the convenient reusable procedure due to the added FeOx, the 2,4-DCP removal performance is still acceptable compared to non-magnetically separable TiO_2/POM(1%) within 180 min. The 2,4-DCP-degradation observed in the dark was due to the 2,4-DCP-adsorption on the TiO_2/FeOx(25%)/POM(1%) surface amounting to 2.1%. Furthermore, runs were carried out depositing POM on TiO_2 followed by the deposition of FeOx leading to the TiO_2/POM(1%)/FeOx(25%). The 2,4-DCP kinetics did not change when the incorporation sequence of FeOx and POM was changed and varied only by 4.5%. It suggests that FeOx and POM were deeply buried in the lattice of TiO_2.

The extent of mineralization of 2,4-DCP was determine by total organic carbon (TOC) and the results shown in Fig. 2. TOC removed of 55.9% was observed in the presence of TiO_2/FeOx(25%)/POM(1%), while 34.9%, 42.8%, 73.1% removal were obtained on bare TiO_2, TiO_2/FeOx(25%) and TiO_2/POM(1%) respectively. The TOC reduction of TiO_2/POM(1%) was higher than the one observed for TiO_2/FeOx (25%)/POM(1%). The 2,4-DCP was not fully mineralized due to long-lived intermediates formed in solution resistant to the attack of: a) the photo-generated ROS and b) the TO_2 photo-generated holes.

The stability of TiO_2/FeOx(25%)/POM(1%) was evaluated by its reusability and Fe-ions leaching experiment during 2,4-DCP degradation. After each cycle, the catalyst was collected from the solution by an external magnet. The catalyst collected on the magnet was washed with de-ionized water and ethanol and dried at 70 °C for 1 h. Fig. 3 shows the cyclic photo-degradation of 2,4-DCP. It is readily seen from Fig. 3 that 58.2% 2,4-DCP removal was achieved after the fifth recycling with respect to the first cycle 75.9%. The stability of the catalyst was further investigated by following the leaching of the Fe-ions during 2,4-DCP-degradation mediated by TiO_2/FeOx(25%)/POM(1%) using the Ferrozine method [34]. The results are displayed in Fig. 4. The total concentration of Fe-ions (Fe^{2+} + Fe^{3+}) was 50–70 μg/L in the ppb level within 180 min as shown in Fig. 4. It suggests that Fe- ions leaching was negligible. The initial concentration of Fe^{3+}-ions was several orders of magnitude higher compared to the Fe^{2+}-ions in solution. The level of Fe^{2+}-ions in the end of the reaction was higher relative to the Fe^{3+}-ions, since the reaction rate Fe^{3+} to Fe^{2+} (k_1 = 76 $M^{-1}s^{-1}$) is much faster compared to the reaction rate Fe^{2+} to Fe^{3+} (k_2 = 0.02 $M^{-1}s^{-1}$) [35].

Figure S3 shows the high-pressure liquid chromatography (HPLC) spectrum observed during 2,4-DCP-degradation mediated by TiO_2/FeOx(25%)/POM(1%) photocatalyst. The retention time of ˜5.2 min. Small additional peaks appeared with time in the HPLC-spectrogram, indicating that long-lived degradation intermediates were generated during 2,4-DCP-degradation. This is consistent with the observed TOC result.

3.2. Effects of the initial 2,4-DCP concentration, catalyst concentration, solution pH, light intensity (fluence rate) and radical intermediates intervening during the 2,4-DCP-removal

In the supplemental Figure S4, the 2,4-DCP-degradation shows a slower kinetics when the concentration of 2,4-DCP was increased following the known pattern of heterogeneous catalytic reactions. The

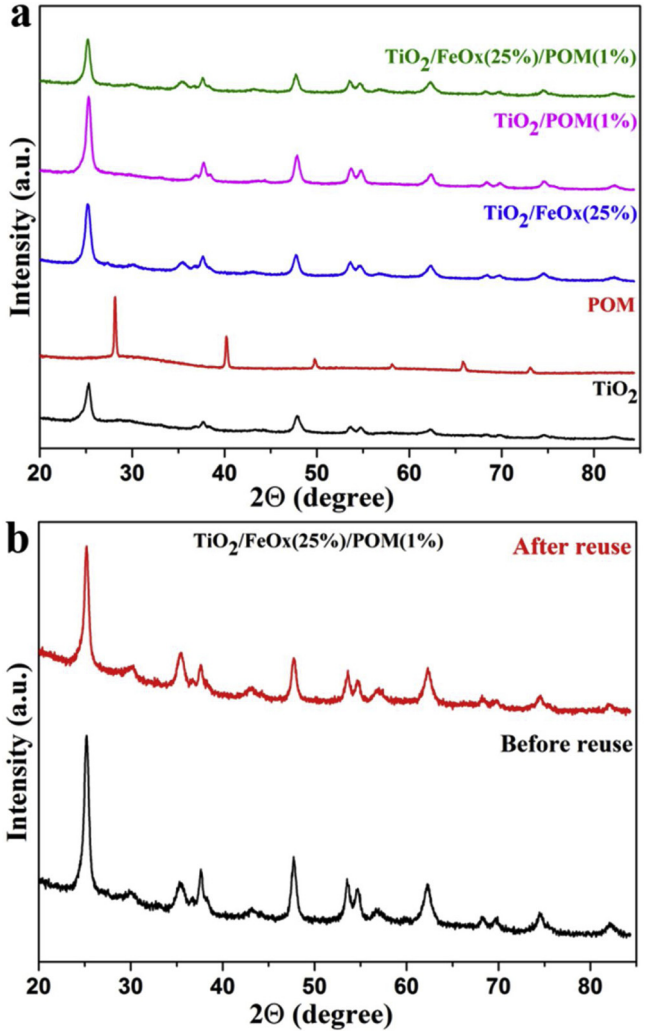

Fig. 10. (a) XRD pattern of photocatalysts used during this study at time zero); (b) XRD pattern of TiO_2/FeOx(25%)/POM(1%) before and after five recycling times.

Table 1
Summary of average crystallite size for each component in different photocatalysts calculated from the strongest peak signal. (*ND: non-detected*).

Sample	TiO_2 (nm)	POM (nm)	Fe_2O_3 (nm)
POM		40.50	–
TiO_2	15.78	–	–
FeO_x(25%)/TiO_2	13.43	–	12.44
POM(1%)/TiO_2	14.91	ND	–
TiO_2/FeO_x(25%)/POM(1%) (time zero)	15.25	ND	18.3
TiO_2/FeO_x(25%)/POM(1%) (after reuse)	15.65	ND	11.51

supplemental Figure S5 shows the beneficial effect of increasing the catalyst concentration up to 500 mg/L on the 2,4-DCP-degradation kinetics due to the increase of catalytic sites. However, excess catalyst concentration will screen the light penetration in solution, thus decreasing the photocatalytic efficiency.

Fig. 5 presents the results of 2,4-DCP-degradation mediated by TiO_2/FeOx(25%)/POM(1%) in the solution pH range of 3–11 considering the most common values reported in the literature. The best condition for 2,4-DCP-degradation was found at initial pH 5. 2,4-DCP presents one pKa value at ~7.9 [36]. When the solution initial pH = 5, the 2,4-DCP is present in an amphoteric form. TiO_2 has an IEP of about 6.2–7.5 [37]. The TiO_2 based photocatalysts prepared in this study are positively charged at $pH_{initial}$ at 5 and will undergo electrostatic attraction with the 2,4-DCP-anionic negative group enhancing the 2,4-DCP-degradation. Table S1 shows the initial (after adding the catalyst to the solution) and final pH values (after the 2,4-DCP degradation under solar simulated light) using TiO_2, TiO_2/FeOx(25%), TiO_2/POM (1%) and TiO_2/FeOx(25%)/POM(1%).

Fig. 6 shows the effect of light intensity (fluence rate) on the DPC degradation kinetics mediated by TiO_2/FeOx(25%)/POM(1%) under simulated solar light. A lower light dose led to slower 2,4-DCP-degradation kinetics due to a lower amount of charges generated in the semiconductor. The 2,4-DCP degradation proceeded also at a low light dose of 4.6 mW/cm^2 (about 10% of AM1).

To understand the photocatalytic mechanism of 2,4-DCP-degradation mediated by TiO_2/FeOx(25%)/POM(1%), ROS trapping experiments were performed using methanol as ·OH scavenger, p-benzoquinone as $\cdot O_2^-$ scavenger, NaN_3 as $^1O_2$ scavenger and potassium iodine KI as hole scavenger. A concentration of 0.5 mM scavenger was used. The results are shown in Fig. 7 showing that the 2,4-DCP-degradation efficiency decreased from 80% to 4% and 17% with methanol and p-benzoquninone, respectively. The ·OH and $\cdot O_2^-$ were the main-radicals leading to 2,4-DCP-degradation mediated by TiO_2/FeOx(25%)/POM (1%). A slight reduction in degradation rate of 2,4-DCP after the introduction of NaN_3 suggests that $^1O_2$ played a minor role in degradation. However, it is noticed that the addition of KI had almost no influence on 2,4-DCP degradation. This shows that h^+ had little effect on the 2,4-DCP-degradation. The ·OH and $\cdot O_2^-$ species are shown to be the main species leading to 2,4-DCP-degradation.

3.3. Diffuse reflectance spectroscopy (DRS) and changes of pH and surface potential during 2,4-DCP degradation

The optical properties of TiO_2-based materials prepared during the course of this study were investigated by diffused reflectance spectroscopy (DRS). The results are presented in Fig. 8a. The samples exhibit an absorption band starting at 250 nm. Compared with TiO_2, TiO_2/FeOx(25%) exhibits absorption both in UV and visible regions because FeOx absorbs visible light up to 535 nm. TiO_2/POM(1%), shows an enhanced absorption in UV region due to the POM presenting a band-gap of ~3.5 eV, similar to the TiO_2 in light absorption. As a result, TiO_2/FeOx(25%)/POM(1%) displays enhanced absorption in the UV and visible regions. The optical band-gap for each catalyst was calculated by the Tauc's method: $\alpha h\nu = B(h\nu\text{-}Eg)^n$, where α is the absorption coefficient, h represents for the Planck's constant, ν the light frequency, B a constant and Eg the band-gap. The value of n depends on whether the transition is direct or indirect, with n = 1/2 for direct transition and n = 2 for indirect transition. Fig. 8b shows that TiO_2, TiO_2/FeOx(25%), TiO_2/POM(1%) and TiO_2/FeOx(25%)/POM(1%) with binding energies of 3.08 eV, 2.75 eV, 3.20 eV and 2.65 eV, respectively. The band gap of TiO_2/FeOx(25%)/POM(1%) was narrowed due to the incorporation of FeOx. It has been recently reported that FeOx intra-gap states facilitate indirect transitions enhancing the light absorption in the visible range [28,38,39].

After the 2,4-DCP degradation, the catalyst recovery is a crucial step. Many catalysts reported in the literature suffer from the nanometric size hindering their recovery. The design of magnetically separable catalysts/photocatalysts showing micrometric sizes helps to overpass the onerous post-treatment costs [39,40]. The TiO_2/FeOx (25%) and TiO_2/FeOx(25%)/POM(1%) samples are paramagnetic showing saturation behavior. The application of an external magnetic field was able to attract the catalysts against the wall of the used flask/reactor. The magnetization level detected in the sample TiO_2/FeOx (25%) was about a 12 times smaller compared to the TiO_2/FeOx(25%)/POM(1%) samples. This suggests the development of hybrid magnetic-catalytic waves/domains that require deeper investigation. This aspect is not the focus of the present study.

The subatomic short-lived excitons, bosons, quarks, mesons making

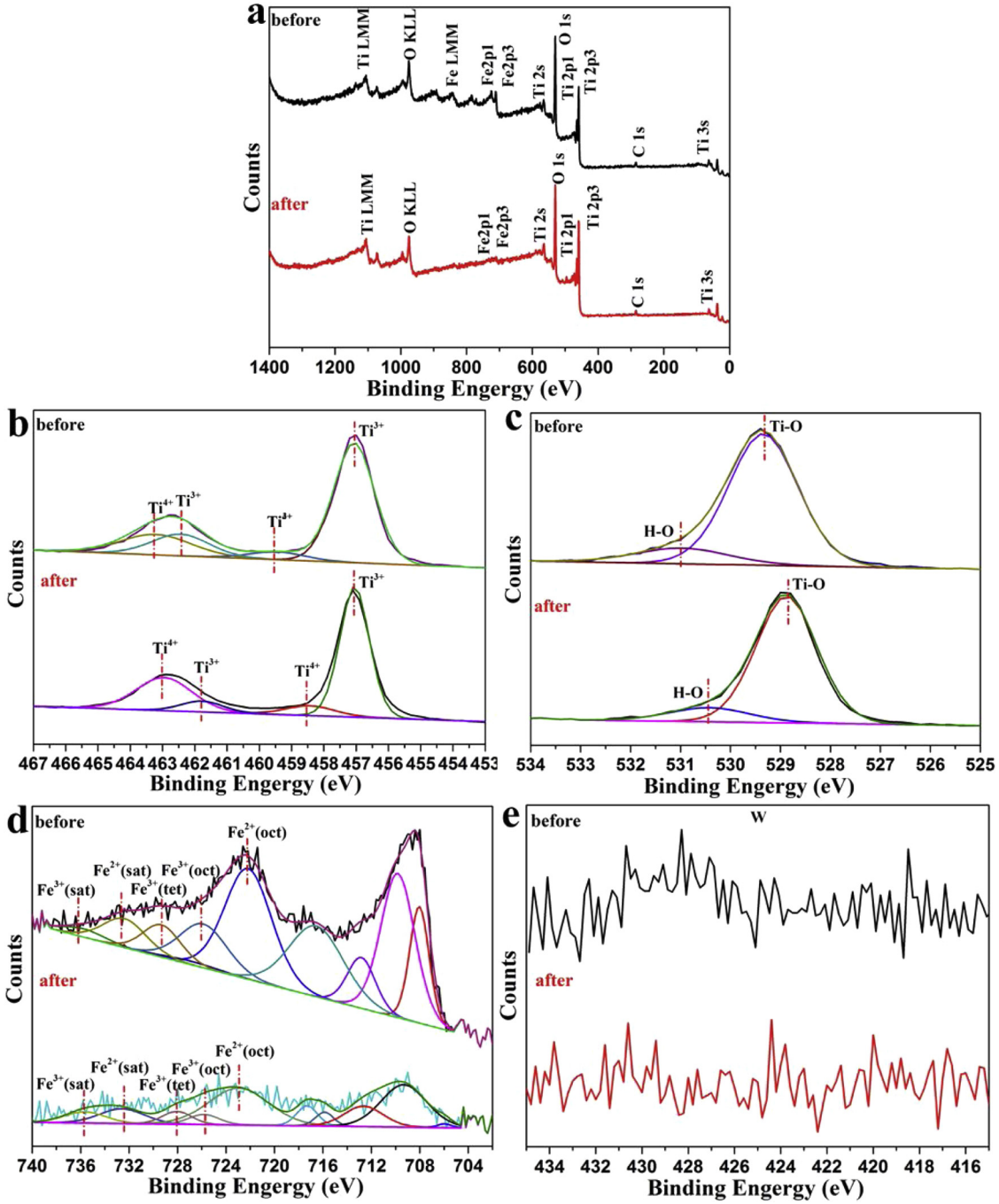

Fig. 11. (a) XPS survey spectrum of TiO_2/FeOx(25%)/POM(1%), (b) Ti2p, (c) O1 s, (d) Fe2p and (e) W4p high resolution spectra of TiO_2/FeOx(25%)/POM(1%) before and after reuse.

up the atoms interaction with the photons/light has been suggested to proceed at a speed higher compared to the speed of light [41–43]. Photons arriving on the catalyst surface disturb the electrons distribution in the atomic and subatomic particles [43–45]. The addition of Fe acquire a small random magnetization in random directions but add to zero total magnetization. However, Fe-addition led to an increase of the oscillations in the metal/oxide electrons accompanied by heat effects as recently reported by Yu et al. [28]. In addition, the Fe addition can play the role of intra-gap state leading to increased electron/hole lifetime and subsequently to reduced photo-generated charges recombination. Based on the oxygen content in the prepared composite, it was reported that cation vacancies govern cations diffusion during the preparation (at high temperature). At high oxygen activities and that at low oxygen activities, cation interstitials form [46].

3.4. Morphology and structural characterization of TiO_2/FeOx(25%)/POM(1%) by SEM, BET and XRD

The morphology of the as-prepared samples is investigated by SEM. Fig. 9a shows the large TiO_2 agglomerates presenting diameter of several microns. After decorating with POM, nanopores and micropores were formed on the surface of TiO_2 agglomerates, as shown in Fig. 9b. For TiO_2/FeOx(25%), the TiO_2 agglomerates were smaller and macropores were observed between particles. The morphology of TiO_2/FeOx (25%)/POM(1%) was quiet similar with that of TiO_2/FeOx(25%), as indicated in Fig. 9d. The addition of FeOx in the TiO_2 or TiO_2/POM

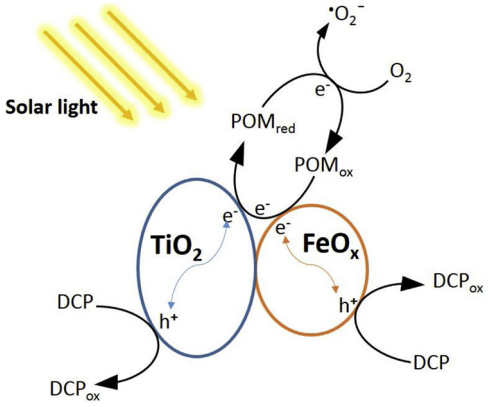

Scheme 2. Simplified 2,4-DCP degradation mechanism on the TiO_2/FeOx (25%)/POM(1%) composite suggesting the IFCT between the three semiconductors.

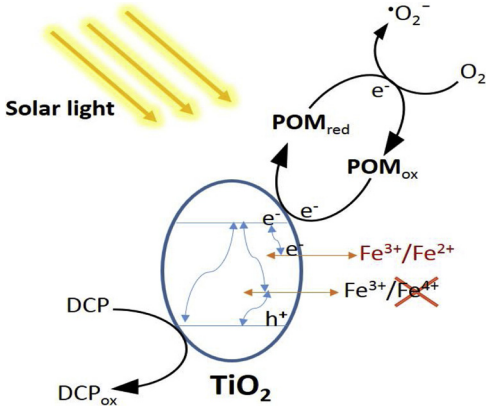

Scheme 3. Simplified 2,4-DCP degradation mechanism on the TiO_2/FeOx (25%)/POM(1%) composite involving Fe-intra-gap states.

(1%) samples does not lead to any modification of the overall size and shape of the material as shown in Fig. 9. Specific surface areas of micro-sized TiO_2, TiO_2-POM, TiO_2-FeOx and TiO_2/FeOx(25%)/POM(1%) are respectively 19.2, 33.09, 37.6 and 48.31 $m^2 g^{-1}$.

Fig. 10a presents the XRD pattern of the different catalysts. The XRD peaks of TiO_2 could be indexed to the anatase TiO_2 (JCPDS card No.21-1272). No additional crystalline phases were detected. Small FeOx peaks at 30.28°, 35.68° and 62.94° were observed in the TiO_2/FeOx (25%) and TiO_2/FeOx(25%)/POM(1%) composites and were attributed to maghemite (JCPDS card No.25-1402). The peaks of POM were not noticeable in the TiO_2/POM(1%) and TiO_2/FeOx(25%)/POM(1%) samples. The POM content in these catalysts was beyond the detection limit of the XRD instrument. By using the Debye-Scherrer equation [28,38] it was possible to estimate a crystallite size for TiO_2 using the (101) reflections and FeOx using the (119) reflections. Table 1 shows the sample crystallite sizes for TiO_2, POM and FeOx. The crystallite sizes of TiO_2, TiO_2/FeOx(25%), TiO_2/POM(1%) TiO_2/FeOx(25%)/POM (1%) and reused TiO_2/FeOx(25%)/POM(1%) were found to be 15.78 nm, 13.43 nm, 14.91 nm, 15.25 nm and 15.65 nm respectively. The reduction in the TiO_2 size compared to pure TiO_2 was probably due its increased compactness and Ti^{4+} substitution by Fe^{3+} during the calcination step. This observation is consistent with the SEM data. Fig. 10b shows the XRD pattern of TiO_2/FeOx(25%)/POM(1%) before and after 5 cycles. The intensity of the peaks on Fig. 10b were reduced by ~13% after five cycles and shows a relative high stability for the TiO_2/FeOx(25%)/POM(1%).

3.5. XPS characterization of TiO_2/FeOx(25%)/POM(1%)

The surface composition and chemical states of the elements present in TiO_2/FeOx(25%)/POM(1%) before and after 2,4-DCP degradation were investigated by XPS, as shown in Fig. 11. The survey XPS spectrum of TiO_2/FeOx(25%)/POM(1%) is shown also in Fig. 11a. The surface atomic ratio of Fe in TiO_2/FeOx(25%)/POM(1%) before and after 2,4-DCP degradation were detected to be 6.29% and 1.31%, respectively. Fig. 11b shows the peaks at 464.2 eV and 458.5 eV for Ti $2p_{1/2}$ and Ti $2p_{3/2}$, respectively. The O 1s region of TiO_2/FeOx(25%)/POM(1%) in Fig. 11c was deconvoluted into two peaks at 535.4 eV and 529.9 eV ascribed to −OH and Ti−O, respectively. The Fe3d XPS spectra of TiO_2/FeOx(25%)/POM(1%) before and after reuse is shown in Fig. 11d. At time zero, the sample BE was 722.3 eV due to Fe^{2+} (oct) species, with a satellite (sat) peak at 732.6 eV. The peaks at 726.1 eV and 729.3 eV correspond to the Fe (oct) and Fe (tet) species, with a corresponding satellite at 736.2 eV. The atomic ratio of Fe^{2+}/Fe^{3+} varied after sample reuse, and this suggests *redox* catalysis taking place during the 2,4-DCP degradation. Fig. 11e shows that the XPS high resolution peaks of W4p before and after reuse did not present. This is due to the extremely low content of W in TiO_2/FeOx(25%)/POM(1%). The C1s content increased slightly after the photocatalytic 2,4-DCP degradation. This can be

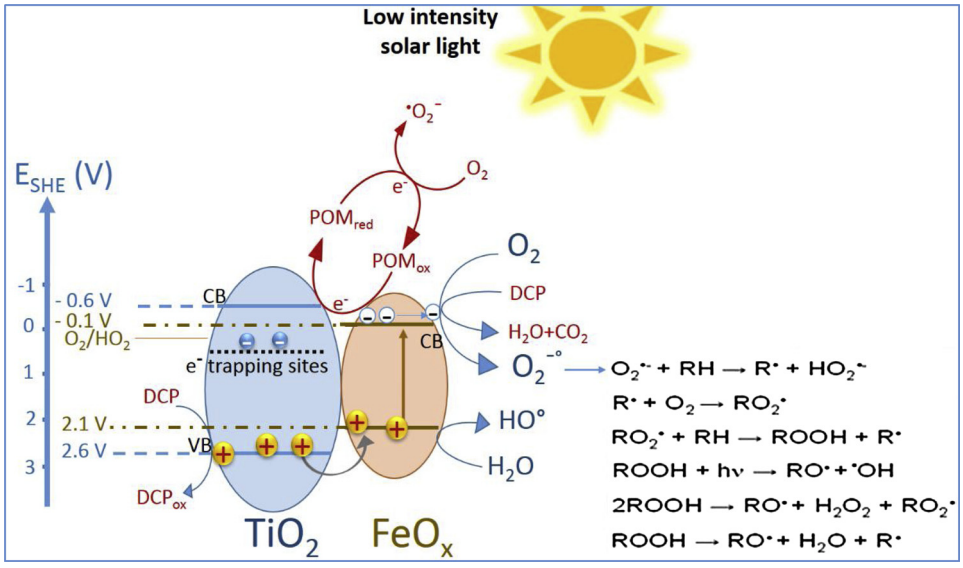

Fig. 12. A mechanism suggested for 2,4-DCP degradation on the TiO_2/FeOx(25%)/POM(1%) composite.

attributed to the adsorption of the photogenerated intermediates, however, the C1 s increase did not reach 5%.

3.6. Suggested interfacial charge transfer in TiO_2/FeOx(25%)/POM(1%) leading to 2,4-DCP degradation under solar simulated light

W-based POM is an important class of photocatalytic materials that is attracting a lot of attention due to their poly-anionic structure and oxidative stability. The photocatalytic activity of these compounds is based on the charge transfer from oxygen to the metal (here tungsten). The main spectral absorbance of this compound is in the near-UV region but the interfacial charge transfer mechanism (IFCT) for the TiO_2/FeOx (25%)/POM(1%) sample under solar light (with its small UV-component) Is suggested in Scheme 2. The formation of a semiconductor-semiconductor heterojunction decreases the rate of photo-generated charges recombination by yielding long-lived electron-hole pairs [47].

The mechanism suggesting the formation of Fe-intra-gap states is presented in Scheme 3. It has been widely reported that metallic dopants introduce additional energetic levels in the band gap of the doped semiconductor. This allows the reduction of the energy barrier and leads to narrower optical absorption edge [47,48]. Scheme 3 shows the photocatalytic activity enhancement in of Fe-doped TiO_2 proceeding through Fe^{3+}/Fe^{4+} as hole-trap centers and Fe^{2+}/Fe^{3+} as electron-trap centers [49,48]. However, from the XPS results, Fe^{4+} was not observed. This excludes the possible hole trapping centers pathway. In addition, Lee et al., reported on the high instability of the redox couple Fe^{3+}/Fe^{4+} [50].

Fig. 12 presents the detailed mechanism of 2,4-DCP degradation on TiO_2/FeOx(25%)/POM(1%) composite based on our findings and material characterization. Note that all the potential values reported in this section are with respect to the standard hydrogen electrode (SHE). The redox potentials of the 2,4-DCP solution (pH = 7.0) were referenced by the Nernst equation: $E^{\Theta}(\text{pH}) = E^{\Theta}(\text{pH} = 0) - 0.059\text{xpH}$ except that $O_2/\cdot O_2^-$ has a potential of -0.33 eV and is pH independent.

The mechanism of action of the poly-oxo-tungstate (POM) can be summarized as follow:

$$\text{POM} \xrightarrow{h\nu} \text{POM}(e^-/h^+)$$

$$\text{POM}(e^-/h^+) + H_2O \rightarrow \text{POM}(e^-) + {}^{\bullet}OH^+$$

$$\text{POM}(e^-) + O_2 \rightarrow \text{POM} + O_2^-$$

$$\text{POM}(e^-/h^+) + \text{DCP} \rightarrow \text{POM}(e\text{-}) + \text{DCP}^{\bullet +}$$

$${}^{\bullet}O\,H + \text{DCP} \rightarrow \text{DCP} - OH^{\bullet} \leftrightarrow \text{DCP}^{\bullet +} + OH^-$$

The mechanism of 2,4-DCP degradation on TiO_2-FeOx can be suggested as follow:

$$O_2^{\bullet -} + H^+ \rightarrow HO_2^{\bullet}$$

$$\text{FeOx} \xrightarrow{h\nu} \text{FeOx}(e^-/h^+)$$

$$\text{FeOx}(h^+) + OH^- \rightarrow {}^{\bullet}OH$$

$$\text{FeOx}(h^+) + H_2O \rightarrow {}^{\bullet}OH + H^+$$

$$\text{FeOx}(e^-) + TiO_2 \rightarrow \text{FeOx} + TiO_2(e^-)_{\text{trapping sites}}$$

$$\text{FeOx}(e^-) + O_2 \rightarrow \text{FeOx} + O_2^-$$

$$\text{DCP}^{\bullet} + O_2 \rightarrow \text{DCP}^{\bullet} + O_2^{\bullet -}$$

$$O_2^{\bullet -} + H^+ \rightarrow HO_2^{\bullet} \Rightarrow \text{other ROS}$$

$$TiO_2(e^-) + O_2 \rightarrow TiO_2 + O_2^-$$

$$TiO_2(h^+) + \text{DCP} \rightarrow CO_2 + H_2O + \text{intermediates}$$

The mechanism involving the three semiconductors is more complex and can be simplified as follow:

$$\text{DCP} + [TiO_2(e^-/h^+) + \text{FeOx}(e^-/h^+)] + h\nu \rightarrow [\text{DCP} + \text{FeOx}^{\bullet} + TiO_2] \rightarrow [\text{DCP}^{\bullet} + \text{FeOx} + TiO_2\text{exciplex}] \rightarrow [\text{DCP}^{\bullet} + \text{FeOx} + TiO_2(\text{exciplex})] \rightarrow CO_2 + H_2O + \text{intermediates}$$

The photocatalytic efficiency reported in this study is aligned with previous studies reporting on the degradation of 2,4-DCP. Chen et al., [51] showed that the process of UV/Persulfate was effective to remove 2,4-DCP in actual water body within 30 min following a first-order kinetic. Within few hours, Yin et al. [52], degraded 2,4-DCP by sequential visible-light driven photocatalysis and Laccase catalytic membrane. Polydivinylbenzene-supported zinc phthalocyanine was reported efficient to photocatalytically degrade and partially mineralize 2,4-DCP in the presence of air or H_2O_2 under halogen lamp illumination within 360 min [53]. The advantages of the magnetically separable photocatalyst used in our study are: (i) the direct contact between the pollutant and the catalyst in suspension, (ii) the stability of the used photocatalysts as shown during cyclic reuses, and (iii) the possibility to recover them after for storage and/or subsequent reuse [28,39].

4. Conclusions

This work provides the evidence for magnetically separable TiO_2-based photocatalyst leading to an accelerated 2,4-DCP-degradation. Non-magnetic TiO_2/POM(1%) led to the fastest 2,4-DCP degradation kinetics with 87.6% compared to magnetically separable TiO_2/FeOx (25%)/POM(1%) leading to 76% 2,4-DCP degradation within 180 min under simulated solar light at pH 5.0. The 2,4-DCP-degradation observed in the dark was due to the 2,4-DCP-adsorption on the TiO_2/FeOx (25%)/POM(1%) surface amounting to 2.1%. TOC removed of 55.9% was observed in the presence of TiO_2/FeOx(25%)/POM(1%), while 34.9%, 42.8%, 73.1% removal were obtained on bare TiO_2, TiO_2/FeOx (25%) and TiO_2/POM(1%) respectively. The addition of FeOx was seen to extend the visible light absorption of the wide band-gap TiO_2. Evidence is presented for the favorable effect of TiO_2-FeOx intra-gap states accelerating 2,4-DCP-degradation. By the use of appropriate scavengers O_2^- and OH were identified as the main intermediates species leading to 2,4-DCP-degradation. Based on the potential band positions of TiO_2 and FeOx, the possible photocatalytic mechanisms were discussed in detail. A generic mechanism is then suggested for the interfacial charge transfer (IFCT) between the oxide semiconductors leading to 2,4-DCP-degradation under low intensity solar light. Magnetic separation by TiO_2/FeOx(25%)/POM(1%) composite presents advantages over conventional processes reducing the cost associated with the photocatalyst separation after 2,4-DCP-degradation.

Appendix A. Supplementary data

Supplementary material related to this article can be found, in the online version, at doi:https://doi.org/10.1016/j.apcatb.2019.04.088.

References

[1] M.A. Zanjanchi, A. Ebrahimian, M. Arvand, Sulphonated cobalt phthalocyanine–MCM-41: an active photocatalyst for degradation of 2, 4-dichlorophenol, J. Hazard. Mater. 175 (2010) 992–1000.
[2] E. Brillas, J.C. Calpe, J. Casado, Mineralization of 2, 4-D by advanced electrochemical oxidation processes, Water Res. 34 (2000) 2253–2262.
[3] S. Sabhi, J. Kiwi, Degradation of 2, 4-dichlorophenol by immobilized iron catalysts, Water Res. 35 (2001) 1994–2002.
[4] N.R. Hendricks, T.T. Waryo, O. Arotiba, N. Jahed, P.G. Baker, E.I. Iwuoha, Microsomal cytochrome P450-3A4 (CYP3A4) nanobiosensor for the determination of 2, 4-dichlorophenol—an endocrine disruptor compound, Electrochim. Acta 54 (2009) 1925–1931.
[5] S. Chen, R. Yan, X. Zhang, K. Hu, Z. Li, M. Humayun, Y. Qu, L. Jing, Photogenerated electron modulation to dominantly induce efficient 2, 4-dichlorophenol degradation on BiOBr nanoplates with different phosphate modification, Appl. Catal. B: Environ. 209 (2017) 320–328.
[6] M. Pera-Titus, V. García-Molina, M.A. Baños, J. Giménez, S. Esplugas, Degradation of chlorophenols by means of advanced oxidation processes: a general review, Appl.

Catal. B: Environ. 47 (2004) 219–256.
[7] Q. Yang, H. Choi, S.R. Al-Abed, D.D. Dionysiou, Iron–cobalt mixed oxide nanocatalysts: heterogeneous peroxymonosulfate activation, cobalt leaching, and ferromagnetic properties for environmental applications, Appl. Catal. B: Environ. 88 (2009) 462–469.
[8] X.J. Chen, Y.Z. Dai, X.Y. Wang, J. Guo, T.H. Liu, F.F. Li, Synthesis and characterization of Ag3PO4 immobilized with graphene oxide (GO) for enhanced photocatalytic activity and stability over 2, 4-dichlorophenol under visible light irradiation, J. Hazard. Mater. 292 (2015) 9–18.
[9] A. Karci, I. Arslan-Alaton, T. Olmez-Hanci, M. Bekbölet, Transformation of 2, 4-dichlorophenol by H_2O_2/UV-C, Fenton and photo-Fenton processes: oxidation products and toxicity evolution, J. Photochem. Photobiol. A: Chem. 230 (2012) 65–73.
[10] R. Li, X. Jin, M. Megharaj, R. Naidu, Z. Chen, Heterogeneous Fenton oxidation of 2, 4-dichlorophenol using iron-based nanoparticles and persulfate system, Chem. Eng. J. 264 (2015) 587–594.
[11] Y. Wu, H. Wang, W. Tu, Y. Liu, S. Wu, Y.Z. Tan, J.W. Chew, Construction of hierarchical 2D-2D Zn3In2S6/fluorinated polymeric carbon nitride nanosheets photocatalyst for boosting photocatalytic degradation and hydrogen production performance, Appl. Catal. B: Environ. 233 (2018) 58–69.
[12] H. Al-Ekabi, N. Serpone, E. Pelizzetti, C. Minero, M.A. Fox, R.B. Draper, Kinetic studies in heterogeneous photocatalysis. 2. Titania-mediated degradation of 4-chlorophenol alone and in a three-component mixture of 4-chlorophenol, 2, 4-dichlorophenol, and 2, 4, 5-trichlorophenol in air-equilibrated aqueous media, Langmuir 5 (1989) 250–255.
[13] L. Liu, F. Chen, F. Yang, Y. Chen, J. Crittenden, Photocatalytic degradation of 2, 4-dichlorophenol using nanoscale Fe/TiO_2, Chem. Eng. J. 181 (2012) 189–195.
[14] A. Fujishima, K. Honda, Electrochemical photolysis of water at a semiconductor electrode, Nature 238 (1972) 37.
[15] A.L. Linsebigler, G. Lu, J.T. Yates Jr., Photocatalysis on TiO_2 surfaces: principles, mechanisms, and selected results, Chem. Rev. 95 (1995) 735–758.
[16] B. O'regan, M. Grätzel, A low-cost, high-efficiency solar cell based on dye-sensitized colloidal TiO_2 films, Nature 353 (1991) 737.
[17] A. Pearson, H. Zheng, K. Kalantar-zadeh, S.K. Bhargava, V. Bansal, Decoration of TiO_2 nanotubes with metal nanoparticles using polyoxometalate as a UV-switchable reducing agent for enhanced visible and solar light photocatalysis, Langmuir 28 (2012) 14470–14475.
[18] C. Hu, Y. Lan, J. Qu, X. Hu, A. Wang, Ag/AgBr/TiO_2 visible light photocatalyst for destruction of azodyes and bacteria, J. Phys. Chem. B 110 (2006) 4066–4072.
[19] M.R. Elahifard, S. Rahimnejad, S. Haghighi, M.R. Gholami, Apatite-coated Ag/AgBr/TiO_2 visible-light photocatalyst for destruction of bacteria, J. Am. Chem. Soc. 129 (2007) 9552–9553.
[20] A. Dolbecq, P. Mialane, B. Keita, L. Nadjo, Polyoxometalate-based materials for efficient solar and visible light harvesting: application to the photocatalytic degradation of azo dyes, J. Mater. Chem. 22 (2012) 24509–24521.
[21] H. Park, W. Choi, Photo-electrochemical investigation on electron transfer mediating behaviors of polyoxometalate in UV-illuminated suspensions of TiO_2 and Pt/TiO_2, J. Phys. Chem. B 107 (2003) 3885–3890.
[22] R.R. Ozer, J.L. Ferry, Investigation of the photocatalytic activity of TiO_2 – polyoxometalate systems, Environ. Sci. Technol. 35 (2001) 3242–3246.
[23] B. Yue, Y. Zhou, J. Xu, Z. Wu, X. Zhang, Y. Zou, S. Jin, Photocatalytic degradation of aqueous 4-chlorophenol by silica-immobilized polyoxometalates, Environ. Sci. Technol. 36 (2002) 1325–1329.
[24] T. Kasuga, M. Hiramatsu, A. Hoson, T. Sekino, K. Niihara, Formation of titanium oxide nanotube, Langmuir 14 (1998) 3160–3163.
[25] M.T. Pope, G.M. Varga, Heteropoly Blues. I. Reduction stoichiometries and reduction potentials of some 12-tungstates, Inorg. Chem. 5 (1966) 1249–1254.
[26] S.E. Braslavsky, A.M. Braun, A.E. Cassano, A.V. Emeline, M.I. Litter, L. Palmisano, V.N. Parmon, N. Serpone, Glossary of terms used in photocatalysis and radiation catalysis (IUPAC Recommendations 2011), Pure Appl. Chem. 83 (2011) 931–1014.
[27] G. Mamba, J. Kiwi, C. Pulgarin, R. Sanjines, S. Giannakis, S. Rtimi, Evidence for the degradation of an emerging pollutant by a mechanism involving iso-energetic charge transfer under visible light, Appl. Catal. B: Environ. 233 (2018) 175–183.
[28] J. Yu, J. Kiwi, I. Zivkovic, H.M. Rønnow, T. Wang, S. Rtimi, Quantification of the local magnetized nanotube domains accelerating the photocatalytic removal of the emerging pollutant tetracycline, Appl. Catal. B: Environ. 248 (2019) 450–458.
[29] J.P. Nogier, M. Delamar, X-ray photoelectron spectroscopy of TiO_2/V_2O_5 catalysts, Catal. Today 20 (1994) 109–123.
[30] J.F. Moulder, W.F. Stickle, P.E. Sobol, K.D. Bomben, J. Chastain (Eds.), Handbook of X-Ray Photoelectron Spectroscopy, Perkin-Elmer Corporation (Physical Electronics Division), Minnesota, USA, 1992.
[31] D.A. Shirley, High-resolution X-ray photoemission spectrum of the valence bands of gold, Phys. Rev. B 5 (1972) 4709–4714.
[32] K.L. Hardee, A.J. Bard, Photo-electrochemical behavior of several polycrystalline metal oxide electrodes in aqueous solutions, J. Electrochem. Soc. 124 (1977) 215–224.
[33] M. Yousaf, H.M. Rafique, M. Amin, S.M. Ramay, S. Atiq, N.S. Alzayed, S.A. Siddiqi, Visible light induced Fe-doped magnetic photocatalyst nanoparticles for the degradation of methylene blue, J. Nanomaterials and Biostructures 12 (2017) 91–98.
[34] E. Viollier, P.W. Inglett, K. Hunter, A.N. Roychoudhury, P. Van Cappellen, The ferrozine method revisited: Fe(II)/Fe(III) determination in natural waters, Appl. Geochem. 15 (2000) 785–790.
[35] V. Nadtocheko, J. Kiwi, Primary photochemical reactions of the photo-fenton system with ferric chloride, Env. Sci. Technol. 32 (1998) 3273–3281.
[36] M.Z. Alam, S.A. Muyibi, J. Toramae, Statistical optimization of adsorption processes for removal of 2, 4-dichlorophenol by activated carbon derived from oil palm empty fruit bunches, J. Environ. Sci. (China) 19 (2007) 674–677.
[37] M.R. Hoffmann, S.T. Martin, W. Choi, D.W. Bahnemann, Environmental applications of semiconductor photocatalysis, Chem. Rev. 95 (1995) 69–96.
[38] J. Kiwi, S. Rtimi, Mechanisms of the antibacterial effects of TiO_2-FeOx under solar or visible light: schottky barriers versus surface plasmon resonance, Coatings 8 (2018) 391.
[39] M. Mangayayam, J. Kiwi, S. Giannakis, C. Pulgarin, I. Zivkovic, A. Magrez, S. Rtimi, FeOx magnetization enhancing *E. coli* inactivation by orders of magnitude on Ag-TiO_2 nanotubes under sunlight, Appl. Catal. B: Environ. 202 (2017) 438–445.
[40] D. Gumy, P. Fernandez-Ibanez, S. Malato, C. Pulgarin, O. Enea, J. Kiwi, Supported Fe/C and Fe/Nafion/C catalysts for the photo-Fenton degradation of Orange II under solar irradiation, Catal. Today 101 (2005) 375–382.
[41] H.-J. Hochecker, The duality of the mass as a basis of the field-forces, Int. J. Phys. 5 (2017) 121–134.
[42] X.-X. Zhang, T. Cao, Z. Lu, Y.-C. Lin, F. Zhang, Y. Wang, Z. Li, J.C. Hone, J.A. Robinson, D. Smirnov, S.G. Louie, T.F. Heinz, Magnetic brightening and control of dark excitons in monolayer WSe2, Nat. Nanotechnol. 12 (2017) 883–888.
[43] N. Bohr, Resonance in nuclear photo-effects, Nature 141 (1938) 1096–1097.
[44] P. Kofstad, Defects and transport properties of metal oxides, Oxid. Met. 44 (1995) 3–27.
[45] R. Dieckmann, Point defects and transport properties of binary and ternary oxides, Solid State Ion. 12 (1984) 1–22.
[46] S. Aggarwal, R. Dieckmann, Point defects and cation tracer diffusion in $(Ti_x Fe_{1-x})_{3-\delta}O_4$. II. Cation tracer diffusion, Phys. Chem. Minerals 29 (2002) 707–718.
[47] V.J. Babu, S. Vempati, T. Uyar, S. Ramakrishna, Review of one-dimensional and two-dimensional nanostructured materials for hydrogen generation, Phys. Chem. Chem. Phys. 17 (2015) 2960–2986.
[48] T. Jafari, E. Moharreri, A. Shirazi Amin, R. Miao, W. Song, S.L. Suib, Photocatalytic water splitting—the untamed dream: a review of recent advances, Molecules 21 (2016) 900.
[49] S. Piskunov, O. Lisovski, J. Begens, D. Bocharov, Y.F. Zhukovskii, M. Wessel, E. Spohr, C-, N-, S-, and Fe-Doped TiO_2 and $SrTiO_3$ nanotubes for visible-light-Driven photocatalytic water splitting: prediction from first principles, J. Phys. Chem. C 119 (2015) 18686–18696.
[50] E. Lee, D.E. Brown, E.E. Alp, Y. Ren, J. Lu, J.-J. Woo, Ch.S. Johnson, New insights into the performance degradation of Fe-Based layered oxides in Sodium-Ion batteries: instability of Fe^{3+}/Fe^{4+} redox in α-$NaFeO_2$, Chem. Mater. 27 (2015) 6755–6764.
[51] J. Chen, N. Gao, X. Lu, M. Xia, Z. Gu, C. Jiang, Q. Wang, Degradation of 2,4-dichlorophenol from aqueous using UV activated persulfate: kinetic and toxicity investigation, RSC-Adv. 6 (2016) 100056.
[52] L. Yin, Z. Shen, J. Niu, J. Chen, Y. Duan, Degradation of pentachlorophenol and 2,4-Dichlorophenol by sequential visible-light driven photocatalysis and laccase catalysis, Environ. Sci. Technol. 44 (2010) 9117–9122.
[53] L. Wu, A. Li, G. Gao, Z. Fei, S. Xu, Q. Zhang, Efficient photodegradation of 2,4-dichlorophenol in aqueous solution catalyzed by polydivinylbenzene-supported zinc phthalocyanine, J. Molecular Catalysis A: Chemical 269 (2007) 183–189.